ELSEVIER

Volume 180, Number 9, September 2007

JOURNAL OF SOLID STATE CHEMISTRY

www.elsevier.com/locate/jssc

CONTENTS

Abstracted/indexed in BioEngineering Abstracts, Chemical Abstracts, Coal Abstracts, Current Contents/Physics, Chemical, & Earth Sciences, Engineering Index, Research Alert, SCISEARCH, Science Abstracts, and Science Citation Index. Also covered in the abstract and citation database SCOPUS®. Full text available on ScienceDirect®.

Regular Articles

Aluminum speciation and thermal evolution of aluminas resulting from modified Yoldas sols
M. Dressler, M. Nofz, F. Malz, J. Pauli, C. Jäger, S. Reinsch and G. Scholz
page 2409

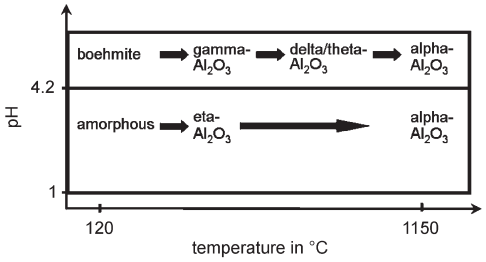

Influence of pH value of parent alumina sols on thermal evolution of resulting xerogels.

Structural and physical properties of $Mg_{3-x}Zn_xSb_2$ ($x = 0$–1.34)
Faraz Ahmadpour, Taras Kolodiazhnyi and Yurij Mozharivskyj
page 2420

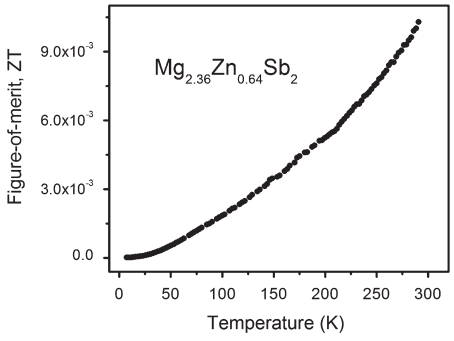

The Mg atoms in Mg_3Sb_2 were successfully substituted with Zn, with Zn going exclusively into the tetrahedral sites. Zn substitution increases the electrical conductivity in $Mg_{2.36}Zn_{0.64}Sb_2$ by closing the band gap. This change combined with a decrease in the thermal conductivity improves the ZT value.

Regular Articles—Continued

Contrasting oxide crystal chemistry of Nb and Ta: The structures of the hexagonal bronzes $BaTa_2O_6$ and $Ba_{0.93}Nb_{2.03}O_6$
W.Gus Mumme, Ian E. Grey, Robert S. Roth and Terrell A. Vanderah
page 2429

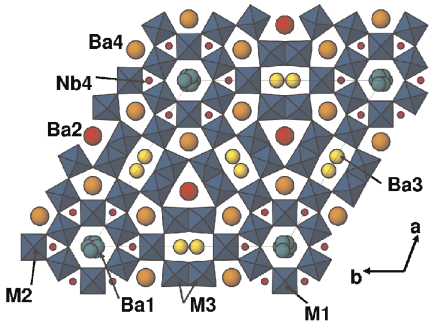

Polyhedral representation of the structure of BaM_2O_6 projected along [0 0 1].

From a 3D protonic conductor $VO(H_2PO_4)_2$ to a 2D cationic conductor $Li_4VO(PO_4)_2$ through lithium exchange
V. Caignaert, M. Satya Kishore, V. Pralong, B. Raveau, N. Creon and H. Fjellvåg
page 2437

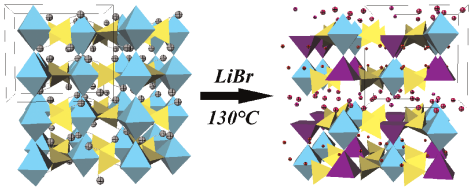

$Li_4VO(PO_4)_2$ was synthesized by a lithium ion exchange reaction from $VO(H_2PO_4)_2$. The structure, determined from neutron and synchrotron powder diffraction data, changes in dimensionality from 3D to 2D. $VO(H_2PO_4)_2$ exhibits a protonic conductivity of 10^{-4} S/cm at room temperature while $Li_4VO(PO_4)_2$ is a lithium conductor.

Energetics of phosphate frameworks containing zinc and cobalt: $NaZnPO_4$, $NaH(ZnPO_4)_2$, $NaZnPO_4 \cdot H_2O$, $NaZnPO_4 \cdot \frac{4}{3}H_2O$, and $NaCo_xZn_{1-x}PO_4 \cdot \frac{4}{3}H_2O$
So-Nhu Le and Alexandra Navrotsky
page 2443

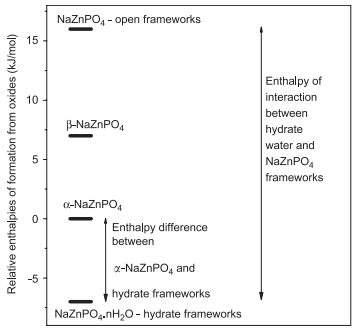

Relative stability of $NaZnPO_4$ dense phases, open frameworks, and hydrated frameworks. Enthalpy of interaction between water and $NaZnPO_4$ frameworks is presented by reaction: $NaZnPO_4$ (cr, open framework) + $n H_2O$ (l) → $NaZnPO_4 \cdot nH_2O$ (cr, hydrated framework).

Rare earth metal-rich indides $RE_{14}Rh_{3-x}In_3$ (RE = Y, Dy, Ho, Er, Tm, Lu)
Roman Zaremba and Rainer Pöttgen
page 2452

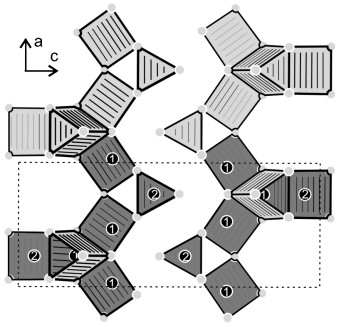

Condensed [RhRE_6] trigonal prisms in $RE_{14}Rh_3In_3$ indides.

Diffusion and reactivity of ZnO–MnO_x system
M. Peiteado, A.C. Caballero and D. Makovec
page 2459

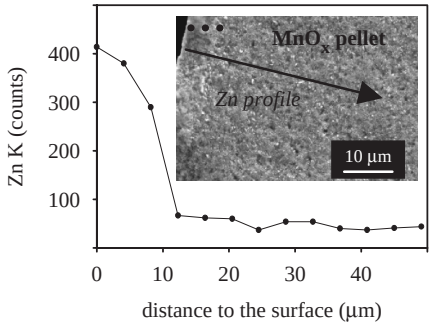

Penetration profile of Zn into MnO_x pellet after firing the ZnO/MnO_x couple at 973 K for 12 h. The formation of a layer of $ZnMn_2O_4$ spinel phase at the surface of MnO_x pellet will impede further diffusion of zinc and manganese species.

Structural arrangements of the ternary metal boride carbide compounds MB_2C_4 (M = Mg, Ca, La and Ce) from first-principles theory
Chang-Ming Fang, Joseph Bauer, Jean-Yves Saillard and Jean-François Halet
page 2465

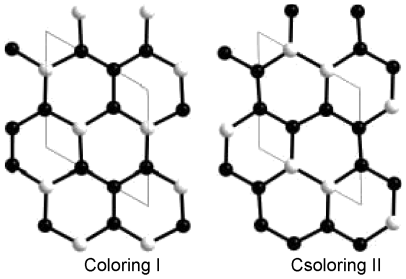

Density-functional theory calculations on the structural arrangements of the ternary metal borocarbides MB_2C_4 (M = Mg, Ca; La and Ce) indicate that these compounds adopt a layered structure consisting of graphite-like B_2C_4 layers alternating with metal sheets. Within the hexagonal layers, the coloring with the –C–C–C–B–C–B– sequence is energetically more stable than that with the –C–C–C–C–B–B– one.

Syntheses, crystal structures and photoluminescence properties of three novel organically bonded indium selenates or selenites
Mei-Ling Feng, Heng-Yun Ye and Jiang-Gao Mao
page 2471

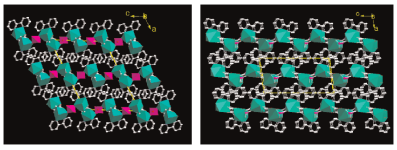

Three new organically bonded indium(III) selenates or selenites hybrids have been synthesized and characterized. Their structures feature organically bonded indium oxalate selenate or selenite layer or hydrogen-bonded 3D structures based on indium selenate dimers.

Thermal and photoluminescence properties of hydrated YPO_4:Eu^{3+} nanowires
Weihua Di, Xiaoxia Zhao, Shaozhe Lu, Xiaojun Wang and Haifeng Zhao
page 2478

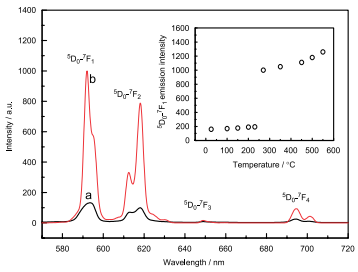

The emission efficiency of the sample annealed at 250 °C is about six times as high as that of as-synthesized sample. This is attributed primarily to the coordinated water as the nonradiative relaxation pathways in the as-synthesized sample.

Continued

Synthesis and CO_2 capture evaluation of $Li_{2-x}K_xZrO_3$ solid solutions and crystal structure of a new lithium–potassium zirconate phase

Mayra Y. Veliz-Enriquez, Gonzalo Gonzalez and Heriberto Pfeiffer

page 2485

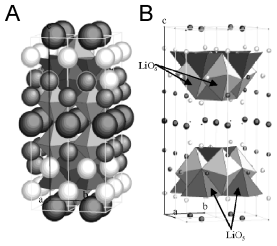

$Li_{2-x}K_xZrO_3$ samples were synthesized and characterized by XRD, SEM, and TGA. The solubility limits of potassium into Li_2ZrO_3 is $x = 0.2$. Additionally, a new phase was synthesized, $Li_{2.27}K_{1.19}Zr_{2.16}O_{6.05}$, which was studied by Rietveld. On the other hand, $Li_{2-x}K_xZrO_3$ solid solutions were tested as CO_2 captors. Analyses showed that $Li_{2-x}K_xZr_2O_3$ samples present a better CO_2 absorption than Li_2ZrO_3 pure.

Quantum efficiency of double activated $Tb_3Al_5O_{12}:Ce^{3+}$, Eu^{3+}

Mihail Nazarov, Do Young Noh, Jongrak Sohn and Chulsoo Yoon

page 2493

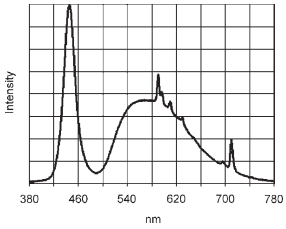

Emission spectra of the blue LED including TAG:Ce, Eu.

Solid state coordination chemistry of the oxofluorovanadium–diphosphonate system in the presence of Cu(II)–tetrapyridylpyrazine complex cations The crystal structures of $[\{Cu_2(tpyprz)(H_2O)_2\}V_4FO_8(HO_3PCH_2PO_3)_2]$, $[\{Cu_2(tpyprz)(H_2O)_2\}V_4F_6O_6(O_3PCH_2CH_2PO_3)]$, and $[Cu_2(tpyprz)\{HO_3P(CH_2)_3PO_3H\}][V_2F_2O_5]$ (tpyprz = tetra-4-pyridylpyrazine)

Wayne Ouellette, Vladimir Golub, Charles J. O'Connor and Jon Zubieta

page 2500

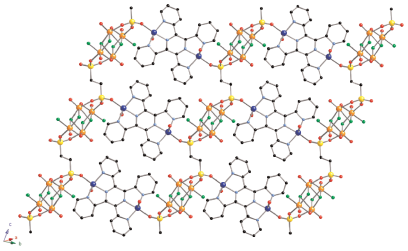

Hydrothermal reactions have been exploited in the preparation of a series of bimetallic oxides constructed from $\{Cu_2(tpyprz)\}^{4+}$ and oxyfluorovanadium organophosphonate components. A view of the two-dimensional structure of the mixed valence $[\{Cu_2(tpyprz)(H_2O)_2\}V_4F_6O_6(O_3PCH_2CH_2PO_3)]$ is provided.

Controlled synthesis of bismuth oxo nanoscale crystals (BiOCl, $Bi_{12}O_{17}Cl_2$, α-Bi_2O_3, and $(BiO)_2CO_3$) by solution-phase methods

Xiang Ying Chen, Hyun Sue Huh and Soon W. Lee

page 2510

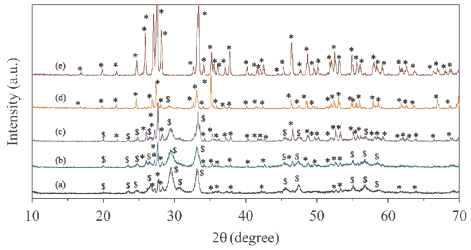

We prepared bismuth oxo nanomaterials by adjusting growth parameters. BiOCl, $Bi_{12}O_{17}Cl_2$, and α-Bi_2O_3 could be prepared from $BiCl_3$ and NaOH, whereas $(BiO)_2CO_3$ was prepared from $BiCl_3$ and urea. BiOCl and $Bi_{12}O_{17}Cl_2$ could also be prepared from $BiCl_3$ and ammonia. The α-Bi_2O_3 sample exhibited strong emission at room temperature.

Characterization of $Bi_5Nb_3O_{15}$ by refinement of neutron diffraction pattern, acid treatment and reaction of the acid-treated product with *n*-alkylamines

Seiichi Tahara, Akira Shimada, Nobuhiro Kumada and Yoshiyuki Sugahara

page 2517

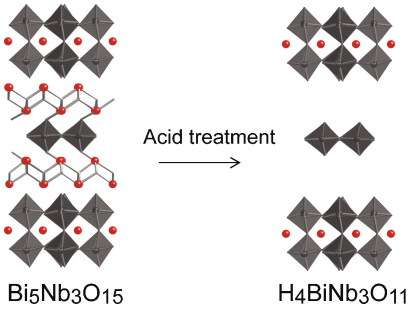

Crystal structure of $Bi_5Nb_3O_{15}$ is investigated by refinement of neutron diffraction pattern as well as by structural change through acid treatment of $Bi_5Nb_3O_{15}$ and subsequent treatment of an acid-treated product with *n*-alkylamine.

Short-time hydrothermal synthesis and delamination of ion exchangeable Mg/Ga layered double hydroxides

Ugur Unal

page 2525

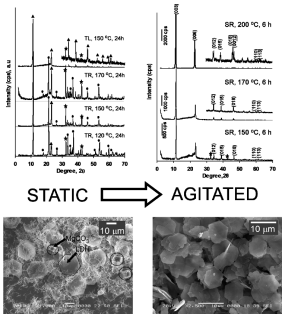

Hydrothermal synthesis under agitation resulted in highly crystalline Mg/Ga LDHs slabs in a short time. The LDHs slabs were delaminated into two-dimensional nanosize sheets.

Copper–indium ordering in $RECu_6In_6$ (RE = Y, Ce, Pr, Nd, Gd, Tb, Dy)
Roman Zaremba, Ihor Muts, Rolf-Dieter Hoffmann, Yaroslav M. Kalychak, Vasyl' I. Zaremba and Rainer Pöttgen
page 2534

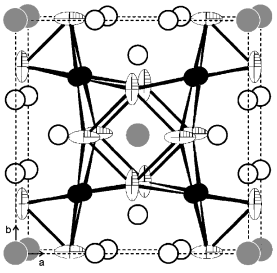

The copper–indium network in $CeCu_6In_6$.

Line patterning of $(Sr,Ba)Nb_2O_6$ crystals in borate glasses by transition metal atom heat processing
M. Sato, T. Honma, Y. Benino and T. Komatsu
page 2541

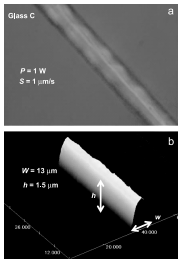

This figure shows the polarization optical (a) and confocal scanning laser (b) micrographs for the sample obtained by heat-assisted (300 °C) Nd:YAG laser irradiation with a laser power of $P = 1$ W and laser scanning speed of $S = 1$ μm/s in Glass C. The figure demonstrates that the transition metal atom heat processing (i.e., a combination of cw Nd:YAG laser and Ni^{2+} ions) is a novel technique for spatially selected crystallization of SBN crystals in glass.

Structure and properties of the $CaFe_2O_4$-type cobalt oxide $CaCo_2O_4$
Mitsuyuki Shizuya, Masaaki Isobe and Eiji Takayama-Muromachi
page 2550

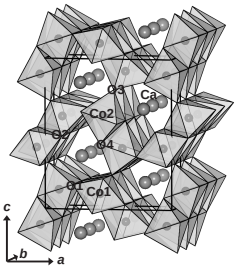

A new calcium cobalt oxide $CaCo_2O_4$ phase, which crystallizes in the calcium-ferrite-type structure (space group: *Pnma*; $a = 8.789(2)$ Å, $b = 2.9006(7)$ Å, and $c = 10.282(3)$ Å), has been synthesized for the first time under high temperature and high pressure (1500 °C, 6 GPa). This compound exhibits large thermoelectric power (Seebeck coefficient: $S = +147$ μV/K at 380 K) and an unsaturated temperature dependence of S around 380 K.

The disordered structures and low temperature dielectric relaxation properties of two misplaced-displacive cubic pyrochlores found in the Bi_2O_3–$M^{II}O$–Nb_2O_5 (M = Mg, Ni) systems
Hai Binh Nguyen, Lasse Norén, Yun Liu, Ray L. Withers, Xiaoyong Wei and Margaret M. Elcombe
page 2558

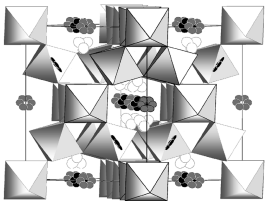

The final displacively disordered average structure of $Bi_{1.667}Mg_{0.70}Nb_{1.52}O_7$ (BMN) projected along a close to ⟨110⟩ direction.

Crystal chemistry and thermodynamic properties of anisotropic $Ce_2Ni_7H_{4.7}$ hydride
R.V. Denys, V.A. Yartys, Masashi Sato, A.B. Riabov and R.G. Delaplane
page 2566

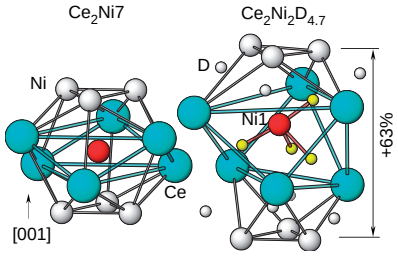

An extremely large volume expansion takes place during the hydrogenation of the hexagonal Ce_2Ni_7 intermetallic compound (left). The expansion proceeds exclusively along one crystallographic direction ([001]) and dramatically modifies the metal sublattice. Hydrogen atoms in $Ce_2Ni_7D_{4.7}$ deuteride form an ordered sublattice and preferably fill sites centred by $NiCe_6$ octahedra (right).

Self-catalyst growth of single-crystalline CaB_6 nanostructures
Junqi Xu, Yanming Zhao, Chunyun Zou and Qiwei Ding
page 2577

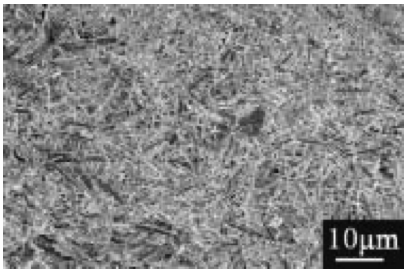

Large-scale calcium hexaboride (CaB_6) nanostructures have been successfully fabricated with self-catalyst method using calcium (Ca) powders and boron trichloride (BCl_3) gas mixed with hydrogen and argon. Our results show that the nanowires are highly single crystals elongated preferentially in the [1 1 0] direction.

Continued

Syntheses, structure, magnetism, and optical properties of the partially ordered quaternary interlanthanide sulfides $PrLnYb_2S_6$ (Ln = Tb, Dy)
Geng Bang Jin, Eun Sang Choi, Robert P. Guertin, James S. Brooks, Corwin H. Booth and Thomas E. Albrecht-Schmitt
page 2581

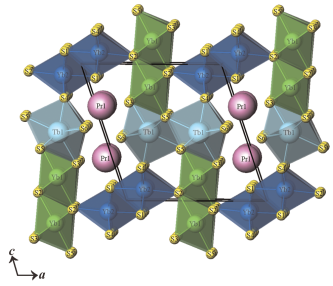

An illustration of the three-dimensional structure of $PrTbYb_2S_6$ viewed along the *b*-axis.

Thermal phase transitions in antimony (III) oxides
R.G. Orman and D. Holland
page 2587

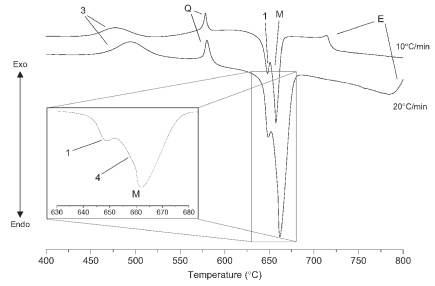

The phase transitions of Sb_2O_3 have been re-examined using XRD and simultaneous TG/DTA, clarifying apparent disagreements in previous works. The thermal events have been detailed, and the α–β phase transition has been observed to occur as a multi-stage event—possibly relating to the presence of surface- or bulk-bound water.

***In situ* ligand synthesis with the UO_2^{2+} cation under hydrothermal conditions**
Mark Frisch and Christopher L. Cahill
page 2597

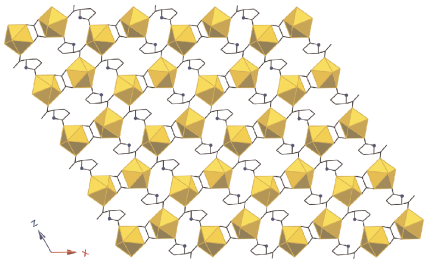

A novel homometallic coordination polymer $(UO_2)_2(C_2O_4)(C_5H_6NO_3)_2$, in the uranium-L-pyroglutamic acid system has been synthesized under hydrothermal conditions. The title compound consists of uranium pentagonal bipyramids bridged through both L-pyroglutamate and oxalate linkages to produce a 3D crystal structure. The oxalate anions are theorized to result from decarboxylation of L-pyroglutamic acid followed by subsequent coupling of CO_2.

Effect of metal doping on the low-temperature structural behavior of thermoelectric β-Zn_4Sb_3
Johanna Nylén, Sven Lidin, Magnus Andersson, Hongxue Liu, Nate Newman and Ulrich Häussermann
page 2603

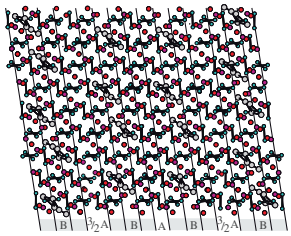

The thermoelectric material Zn_4Sb_3 displays complex temperature polymorphism. Room temperature stable, disordered, β-Zn_4Sb_3 undergoes two phase transitions at 254 and 235 K to the consecutively higher ordered phases α and α', respectively. The α–α' transformation is triggered by a slight and homogenous Zn deficiency and introduces a compositional modulation in the α-Zn_4Sb_3 structure.

Preparation, spectroscopic properties of 1,4-di (*N*,*N*-diisopropylacetamido)-2,3(1*H*,4*H*)-quinoxalinedione (L) lanthanide complexes and the supramolecular structure of $[Nd_2L_2(NO_3)_6(H_2O)_2]\cdot H_2O$
Xue-Qin Song, Yang Yu, Wei-Sheng Liu, Wei Dou, Jiang-Rong Zheng and Jun-Na Yao
page 2616

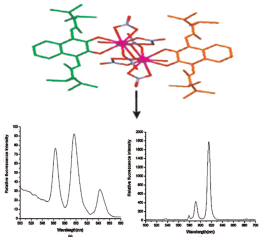

Preparation, spectroscopic properties of 1,4-di (*N*,*N*-diisopropylacetamido)-2,3(1*H*,4*H*)-quinoxalinedione (L) lanthanide complexes and the supramolecular structure of $[Nd_2L_2(NO_3)_6(H_2O)_2]\cdot H_2O$.

Rapid Communications

Continuous nanoparticle production by microfluidic-based emulsion, mixing and crystallization
Y.-F. Su, H. Kim, S. Kovenklioglu and W.Y. Lee
page 2625

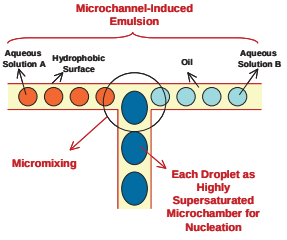

$BaSO_4$ and 2,2′-dipyridylamine (DPA) nanoparticles were synthesized as reactive crystallization and anti-solvent recrystallization examples, respectively, of using the microfluidic-based emulsion and mixing approach as a new avenue of continuously producing inorganic and organic nanoparticles.

New synthesis of excellent visible-light $TiO_{2-x}N_x$ photocatalyst using a very simple method
Danzhen Li, Hanjie Huang, Xu Chen, Zhixin Chen, Wenjuan Li, Dong Ye and Xianzhi Fu
page 2630

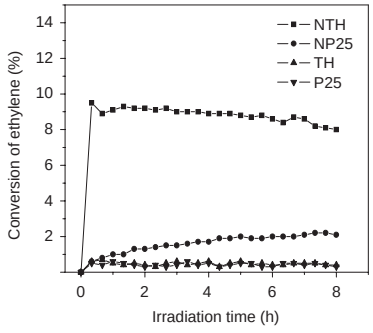

The excellent visible-light-responsive (from 400 to 550 nm) $TiO_{2-x}N_x$ photocatalyst was prepared by a simple wet method. Hydrazine was used as a new nitrogen resource in this paper. In the experiment, a strong photocatalytic activity with high photochemical stability under visible-light irradiation was demonstrated.

Synthesis, characterization and activity of alumina-supported cobalt nitride for NO decomposition
Zhiwei Yao, Aimin Zhu, Jing Chen, Xinkui Wang, C.T. Au and Chuan Shi
page 2635

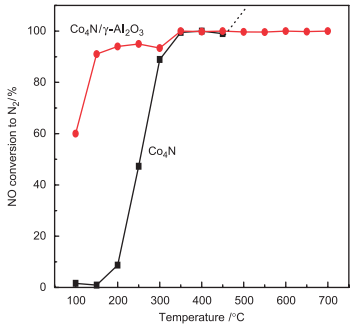

The supported cobalt nitride performs much better than its bulk counterpart for NO decomposition, owing to its small crystal size, high thermal stability and big surface area.

Corrigendum

Corrigendum to "$EuBaFe_2O_{5+w}$: Valence mixing and charge ordering are two separate cooperative phenomena" [J. Solid State Chem. 180 (2007) 148–157]
P. Karen, K. Gustafsson and J. Lindén
page 2641

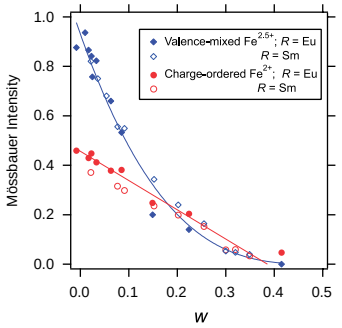

Fraction of $Fe^{2.5+}$ in the valence-mixed state (curve) compared with the fraction of Fe^{2+} in the charge-ordered state (line).

Continued

Author inquiries

Submissions

For detailed instructions on the preparation of electronic artwork, consult the journal home page at http://authors.elsevier.com.

Other inquiries

Visit the journal home page (http://authors.elsevier.com) for the facility to track accepted articles and set up e-mail alerts to inform you of when an article's status has changed. The journal home page also provides detailed artwork guidelines, copyright information, frequently asked questions and more.

Contact details for questions arising after acceptance of an article, especially those relating to proofs, are provided after registration of an article for publication.

Language Polishing

Authors who require information about language editing and copyediting services pre- and post-submission should visit http://www.elsevier.com/wps/find/authorshome.authors/languagepolishing or contact authorsupport@elsevier.com for more information. Please note Elsevier neither endorses nor takes responsibility for any products, goods, or services offered by outside vendors through our services or in any advertising. For more information please refer to our Terms & Conditions at http://www.elsevier.com/wps/find/termsconditions.cws_home/termsconditions.

For a full and complete Guide for Authors, please refer to *J. Solid State Chem.,* Vol. 180, Issue 1, pp. *bmi–bmv*. The instructions can also be found at http://www.elsevier.com/wps/find/journaldescription.cws_home/622898/authorinstructions.

Journal of Solid State Chemistry has no page charges.